equation is correct except for terms of order $\langle e\not{A}\tilde{g}\not{\partial}/mM\rangle$, where $\tilde{g}$ is the BS kernel (or potential). Since the calculations presented in this paper are only to first order in binding, we conclude that minimal coupling of the Breit equation is valid to the accuracy required.

[15]See Eqs. (8) and (9), which are valid expressions even between different eigenstates of $\vec{P}$. In this section we are assuming a scalar nucleus. In the more general case we also write $\langle H_{\rm mag}\rangle$, but if there is nuclear spin, this expectation value does not give the energy shift. Degenerate perturbation theory is needed because of the various total spin states which are possible; this leads to the Breit-Rabi formula. In evaluating expressions like $\langle H_{\rm mag}\rangle$ we are merely evaluating the spatial parts, which for the 1S state are the same regardless of the spin-dependent part of the wave function.

[16]Willis E. Lamb, Jr., Phys. Rev. 85, 259 (1952).

[17]Note that

$$\left[-\frac{Z\alpha}{2M}\left(\frac{1}{r}+i\,\frac{\vec{r}}{r}\cdot p\right)\right]^{\dagger}=-\frac{Z\alpha}{2M}\left(\frac{1}{r}-i\,\vec{p}\cdot\frac{\vec{r}}{r}\right)$$

$$=\frac{Z\alpha}{2M}\left(\frac{1}{r}+i\,\frac{\vec{r}}{r}\cdot\vec{p}\right)\ .$$

[18]S. J. Brodsky and G. W. Erickson, Phys. Rev. 148, 26 (1966).

[19]Alternatively we may calculate this same correction by means of second-order perturbation theory, in which the contribution arises from the product of the radiative and the magnetic interactions. In the lowest-order calculation (nonradiative terms) there are no explicit second-order perturbations, since all terms linear in $\vec{H}$ arise from first-order perturbation theory with the magnetic interaction, using exact eigenfunctions of H, as given by Eq. (4).

[20]N. M. Kroll and F. Pollock, Phys. Rev. 86, 876 (1952).

[21]E. H. Lieb, Phil. Mag. 46, 311 (1955).

[22]The complete Hamiltonian is obtained from Eq. (1) by replacing $\vec{p}_e$ by $\vec{p}_e - e\vec{A}(\vec{x}_e)$ and $\vec{p}_p$ by $\vec{p}_p + Ze\vec{A}(\vec{x}_p)$ as discussed earlier in the paper.

[23]M. H. Johnson and B. A. Lippmann, Phys. Rev. 76, 828 (1949).

[24]W. A. Barker and F. N. Glover, Phys. Rev. 99, 317 (1955).

[25]L. L. Foldy and S. A. Wouthuysen, Phys. Rev. 78, 29 (1950).

[26]Z. V. Chraplyvy, Phys. Rev. 91, 388 (1953); 92, 1310 (1953).

[27]R. Faustov, Phys. Letters 33B, 422 (1970).

[28]F. E. Close and H. Osborn, Phys. Letters 34B, 400 (1971).

PHYSICAL REVIEW A VOLUME 4, NUMBER 1 JULY 1971

Theory of One-Electron Molecules. I. Li_2^+

W. L. McMillan
Bell Telephone Laboratories, Murray Hill, New Jersey 07974
(Received 3 August 1970)

An accurate method for solving the one-electron Schrödinger equation for small molecules is presented. For Li_2^+, the valence-electron-core interaction is treated as an effective potential found by fitting the atomic energy levels. The intermolecular potentials for six low-lying electronic states of Li_2^+ are calculated. For the ground state σ_{g1}, a binding energy of 1.30 eV is found at a separation of 3.08 Å and a vibration frequency of 277 cm^{-1}. From the intermolecular potentials, three cross sections are calculated for Li ions scattering from Li atoms: (i) elastic scattering, (ii) charge transfer, and (iii) inelastic scattering leaving the atom in a $2p$ excited state. This last process proceeds through a curve crossing of the σ_{u1} and π_{u1} states at $R = 5.95a_0$.

I. INTRODUCTION

An accurate and convenient numerical method for solving the one-electron Schrödinger equation for small molecules is presented. This method is applied to the calculation of the intermolecular potentials of six low-lying electronic states of the Li_2^+ molecule. The interaction between the valence electron and the core electrons is treated as an effective potential which is determined by fitting the atomic energy levels of the Li atom. As long as the cores of the Li^+ ions do not overlap appreciably, this effective potential should provide an accurate physical model for Li_2^+. For the ground state σ_{g1}, a binding energy of 1.30 eV is found at an internuclear separation of $R = 5.85a_0$ and a vibration frequency of 277 cm^{-1}.

From the intermolecular potentials we can calculate the cross sections for the three scattering processes that have been studied experimentally: (i) the elastic differential scattering cross section for lithium ions bombarding lithium atoms[1] $Li^+ + Li \rightarrow Li^+ + Li$, (ii) the total charge-transfer cross section[2,3] $Li^+ + Li \rightarrow Li + Li^+$, and (iii) the inelastic differential cross section for the process in which the lithium atom is excited from the $2s$ ground state to the $2p$ state.[1] This last process goes at low energy via a curve crossing of the σ_{u1} and π_{u1} states at $R = 5.95a_0$. We calculate the transition probability $\sigma_{u1} \rightarrow \pi_{u1}$ as a function of ion velocity and impact parameter by integrating the time-dependent Schrödinger equation numerically for

the two-state problem. We can then find the differential cross section for the inelastic process. The elastic and charge-transfer cross sections are computed from the σ_{u1} and σ_{g1} potentials.[4-6] Both of these cross sections are modified by the inelastic process, and these modifications are taken into account. The over-all agreement with the scattering experiments performed thus far is good.

The plan of the paper is as follows: In Sec. II we discuss the one-electron Hamiltonian, and in Sec. III we present the numerical technique for finding the electronic energies and wave functions. In Sec. IV we calculate the intermolecular potentials for the six states derived from the atomic $2s$ and $2p$ states. In Sec. V we calculate the elastic differential cross section in the adiabatic approximation. In Sec. VI we compute the inelastic differential cross section and the corrections to the elastic cross section. In Sec. VII we calculate the charge-transfer cross section.

II. ONE-ELECTRON HAMILTONIAN

The lithium molecular ion has one valence electron, and we can treat the ion as a one-electron problem by replacing the interaction between the valence electron and the core electrons by an effective potential. The effective potential concept should be accurate provided the core electrons are tightly bound compared to the valence electron. We determine the effective potential by taking a one-parameter potential and fitting the atomic energy levels of the lithium atom. We take

$$U_{\text{eff}}(r) = -3/r + (2/r)[1 - (1 + Z_c r)e^{-2Z_c r}], \tag{1}$$

which is the potential of the nucleus plus the Coulomb potential of two core electrons in hydrogenic $1s$ orbitals with effective charge Z_c. With $Z_c = 1.655$, the calculated atomic energy levels (Table I) are in excellent agreement with experiment[7] (atomic units are used throughout). This effective potential should be accurate provided the cores of the two Li^+ ions do not overlap appreciably, that is, for $R > 2a_0$. The one-electron Hamiltonian is then

TABLE I. Comparison with experiment of theoretical energy levels of the lithium atom using the effective potential [Eq. (1)] with $Z_c = 1.655$.

	Experimental energy (a.u.)	Theoretical energy (a.u.)
$2s$	−0.1981	−0.1981
$2p$	−0.1302	−0.1299
$3s$	−0.0742	−0.0743
$3p$	−0.0572	−0.0573
$3d$	−0.0556	−0.0556

$$\mathcal{H} = -\tfrac{1}{2}\nabla^2 + U_{\text{eff}}(|r - R_1|) + U_{\text{eff}}(|r - R_2|), \tag{2}$$

where R_1 and R_2 are the positions of the Li^+ ions. The Schrödinger equation is then

$$\mathcal{H}\psi_n = E_n(R)\psi_n , \tag{3}$$

where the electronic eigenvalue $E_n(R)$ is a function of internuclear separation $R = |\vec{R}_1 - \vec{R}_2|$. The molecule has rotational symmetry about the internuclear axis and a center of symmetry. The wave functions are labeled by the angular momentum about the internuclear axis l, by the inversion symmetry, gerade or ungerade, and by the principal quantum number $n = 1, 2, \ldots$.

The intermolecular potential is the total energy of the molecular ion at separation R minus the energy of the separated Li^+ ion and Li atom:

$$V_n(R) = E_n(R) + V_{\text{ion-ion}}(R) - E_{\sigma_{g1}}(\infty), \tag{4}$$

where

$$V_{\text{ion-ion}}(R) = 1/R + V_{\text{vdW}}(R) + V_{\text{core}}(R). \tag{5}$$

The van der Waals and core-core interactions are determined by scaling the polarizability and He-He interactions[8] by the ratio of characteristic lengths 1.7/2.7 for the Li and the He atom cores:

$$V_{\text{vdW}}(R) = -0.24/(2^4 + R^4), \tag{6}$$

$$V_{\text{core}}(R) = 45e^{-3.85R}, \tag{7}$$

which is Slater's[8] He-He potential properly scaled. These two terms are appreciable only for $R < 3a_0$; they affect only the elastic cross section at large angles (small impact parameters); they have no effect on either the other cross sections or the binding of the molecule.

One can treat the other alkali atoms in the same way as we have treated Li and carry through calculations for all the alkali molecular ions and the alkali-hydride molecular ions. We believe that this model is an accurate physical model for Li_2^+ for $R > 2a_0$ and that calculations based on the model have the same validity as accurate *ab initio* calculations. It is therefore worthwhile to find accurate solutions to the one-electron Schrödinger equation. This problem is considered in Sec. III.

III. SOLVING ONE-ELECTRON PROBLEM

Briefly, the method used to solve the Schrödinger equation is as follows. We write the wave function as a linear combination of convenient functions

$$\psi = \sum_i a_i \varphi_i . \tag{8}$$

Since the potential is Coulombic both near the nuclei and far from the molecule, it is convenient to use Slater functions centered on the nuclei. Since we will deal with excited states, we will not minimize the energy, but will minimize instead

the energy variance $F = \langle (H-E)^2 \rangle$. Minimizing F minimizes the rms error in the solution of the Schrödinger equation and provides an upper limit on the energy error as well as an optimized wave function and eigenvalue. With E fixed, we minimize F with respect to the linear parameters of the wave function and find and eigenvalue equation for F:

$$\sum_j (H_{ij}^2 - 2EH_{ij} + E^2 S_{ij} - FS_{ij}) a_j = 0, \tag{9}$$

where

$$\begin{aligned} S_{ij} &= \int \varphi_i^* \varphi_j d^3r , \\ H_{ij} &= \int \varphi_i^* H \varphi_j d^3r , \\ H_{ij}^2 &= \int (H\varphi_i)^* H \varphi_j d^3r . \end{aligned} \tag{10}$$

Using Slater functions one can easily compute $H\varphi_i$ at a point in space; the integrations are then performed by mesh integration. The eigenvalue equation (9) can be readily solved for the lowest eigenvalue and eigenfunction by standard numerical techniques. One then fixes the wave function and minimizes F with respect to E to find the optimum energy

$$E = \sum_{ij} a_i H_{ij} a_j \Big/ \sum_{ij} a_i S_{ij} a_j = \langle H \rangle . \tag{11}$$

This two-step minimization procedure is iterated until it converges.

If the trial wave function were completely flexible, the energy variance $F(E)$ would vanish at the eigenvalues and rise to the value $\frac{1}{4}(E_i - E_j)^2$ between neighboring eigenvalues. In order to have an accurate solution of the Schrödinger equation we require that $F(E_i) \ll \frac{1}{4}(E_i - E_j)^2$, where $E_i - E_j$ is the energy difference from the closest eigenfunction of the same symmetry. The error function

$$\epsilon = F(E_i)/(E_i - E_j)^2 \tag{12}$$

is a convenient absolute measure of the accuracy of the wave function. One can show that the energy error is less than $\epsilon \times |E_i - E_j|$.

TABLE II. Parameters for the σ_{g1} wave function for $R = 6$. Wave function is not normalized.

a_i	l_i	n_i	A_i
1	0	0	3.5
0.7262	0	0	2.1
−1.4053	0	0	1.3
1.5840	0	0	0.8
−1.0832	0	1	0.8
0.0727	0	2	0.8
0.5619	1	0	2.1
−0.6020	1	0	1.3
0.6238	1	0	0.8
−0.0067	1	1	0.8
0.0189	2	0	1.3
0.0601	2	0	0.8

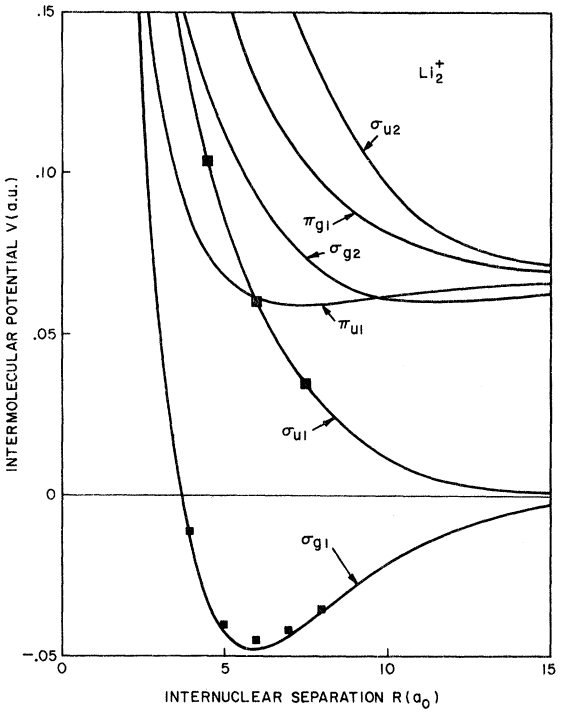

FIG. 1. Intermolecular potentials of six low-lying electronic states of Li_2^+ vs internuclear separation. Solid squares are from the Hartree-Fock-Roothaan calculation by Fisher and Kemmy for the σ_{g1} and σ_{u1} states.

In order to illustrate a typical run we present the calculation of the ground state σ_{g1} at $R = 6a_0$. We take 12 basis functions of the form

$$\varphi_i = z_1^{l_i} r_1^{n_i} e^{-A_i r_1} + z_1^{l_i} r_2^{n_i} e^{-A_i r_2}, \tag{13}$$

and use 130 mesh points to perform the two-dimensional integrals (10). The optimized wave function is given in Table II, the energy is -0.4122, and the energy variance is 1.0×10^{-4}. The energy difference from the next state of the same symmetry is 0.14, so that $\epsilon = 0.0051$, and energy error is less than 0.0007. The intermolecular potential is -0.0474 ± 0.0007, which is near the minimum. The computing time was 20 sec on a GE 635.

IV. ELECTRONIC STATES OF Li_2^+

Using the method described in Sec. III, we have computed the electronic eigenvalues of the six lowest-lying states of Li_2^+ for R between $2a_0$ and $18a_0$. The electronic energies of the σ_{g1}, σ_{u1}, and π_{u1} states, which are of interest for the cross section calculations, are listed in Table III. The intermolecular potentials for six states are plotted in Fig. 1 together with the energies for the σ_{g1} and σ_{u1} computed by Fischer and Kemmey[9] by the Hartree-Fock-Roothaan (HFR) method. The energies for the σ_{u1} state are in excellent agreement; however, the HFR energies for the σ_{g1} state lie

TABLE III. Energy and energy variance of the three lowest electronic states of Li_2^+ as a function of internuclear separation.

	σ_{g1}		σ_{u1}		π_{u1}	
R(a.u.)	E(a.u.)	$F\times10^4$	E(a.u.)	$F\times10^4$	E(a.u.)	$F\times10^4$
2	−0.4746	4.7	−0.3603	0.21	−0.4650	9.7
3	−0.4678	0.9	−0.3394	0.29	−0.4057	4.4
4	−0.4647	1.3	−0.3233	0.26	−0.3628	1.3
5	−0.4413	1.2	−0.3119	0.19	−0.3300	0.56
6	−0.4122	1.0	−0.3043	0.14	−0.3035	0.88
7	−0.3841	1.0	−0.2992	0.12	−0.2817	1.4
8	−0.3593	1.0	−0.2951	0.10	−0.2640	1.7
10	−0.3199	1.1	−0.2868	0.10	−0.2367	1.3
12	−0.2929	0.56	−0.2776	0.13	−0.2177	0.75
15	−0.2684	0.25	−0.2644	0.12	−0.1987	0.39
18	−0.2550	0.11	−0.2541	0.09		

significantly above the energies which we calculate. The largest deviation is 0.006 a.u. = 0.16 eV at $R = 4a_0$. It is not known whether this discrepancy is due to a lack of convergence in the HFR calculation or to some inadequacy of the effective potential. At a separation of $R = 2a_0$ the core states begin to overlap appreciably, and the energy splitting between the σ_g and σ_u core states is about 10% of the core binding energy. As the core wave functions become modified, the effective potential felt by the valence electron should also be modified and the effective potential breaks down. For $R > 2a_0$, however, the model should be accurate.

The ground-state intermolecular potential can be fit by a Morse potential

$$V(R) = V_0(e^{-2\alpha(R-R_0)} - 2e^{-\alpha(R-R_0)}), \tag{14}$$

within ±0.0007 in the attractive region $3.5a_0 < R < 12a_0$. The parameters are $V_0 = 0.048$ a.u., $\alpha = 0.325a_0^{-1}$, $R_0 = 5.82a_0$. This potential yields a binding energy of 1.30 ± 0.02 eV, an equilibrium radius of 3.08 ± 0.05 Å, and a vibrational frequency of 277 ± 8 cm^{-1}.

The curve crossing of the σ_{u1} and π_{u1} states occurs at $R = (5.95 \pm 0.1)a_0$. The π_{u1} states goes to an atomic $2p$ state in the united-atom and separated-atom limits, while the σ_{u1} state goes to an atomic $3p$ state in the united-atom and to an atomic $2s$ state in the separated-atom limit. Thus we expect this level crossing to be characteristic of all the alkali molecular ions, and we expect it to occur at a separation of the order of the size of the atomic wave functions.

V. ELASTIC SCATTERING CROSS SECTION

The elastic differential cross section for the scattering of Li ions by Li atoms has been measured by Aberth *et al.*[1] for center-of-mass energies between 25 and 150 eV. In this section we calculate the elastic cross section within the adiabatic approximation, neglecting the inelastic channel. This calculation is similar to the one by Marchi and Smith[6] for He_2^+. The modifications of the elastic cross section due to the inelastic channel will be computed in Sec. VI.

A. Classical Approximation

The ion motion can be treated classically in this energy range, and we calculate the angle of scattering versus impact parameter using classical perturbation theory. Consider the bombarding ion moving in the z direction with velocity v and impact parameter b. With the electron in the state n, the force on the ion in the x direction is

$$F_x = -\frac{\partial V_n(R)}{\partial x} = -\frac{\partial V_n(R)}{\partial R}\frac{b}{R} = \mu\frac{dv_x}{dt}, \tag{15}$$

where μ is the reduced mass $\frac{1}{2}M_{\mathrm{Li}}$ and v_x is the velocity in the x direction. The scattering angle is then

$$\theta = -\frac{b}{\mu v^2}\int_{-\infty}^{\infty}\frac{dz}{R}\frac{\partial V_n(R)}{\partial R}. \tag{16}$$

In terms of the reduced angle $\tau = E\theta$ the scattering is a function of b alone[10]:

$$\tau(b) \equiv \frac{\mu v^2\theta}{2} = -\frac{b}{2}\int_{-\infty}^{\infty}\frac{dz}{R}\frac{\partial V_n(R)}{\partial R}. \tag{17}$$

If we write the intermolecular potential as a sum of Gaussians, the z integral can be performed, and we find

$$V_n(R) = \sum_i c_i^n e^{-(\alpha_i R)^2}, \tag{18}$$

$$\tau_n(b) = \sqrt{\pi}\, b\sum_i c_i^n\alpha_i e^{-(\alpha_i b)^2}. \tag{19}$$

The coefficients c_i^n are determined by a least-squares fit to the calculated potentials. The differential cross section is

$$\sigma(\theta)\sin\theta\, d\theta = b\,db, \tag{20}$$

and one defines a reduced cross section:

$$\rho_n(\tau) = \theta\sigma(\theta)\ \sin\theta = \frac{\tau_n b}{d\tau_n/db}. \tag{21}$$

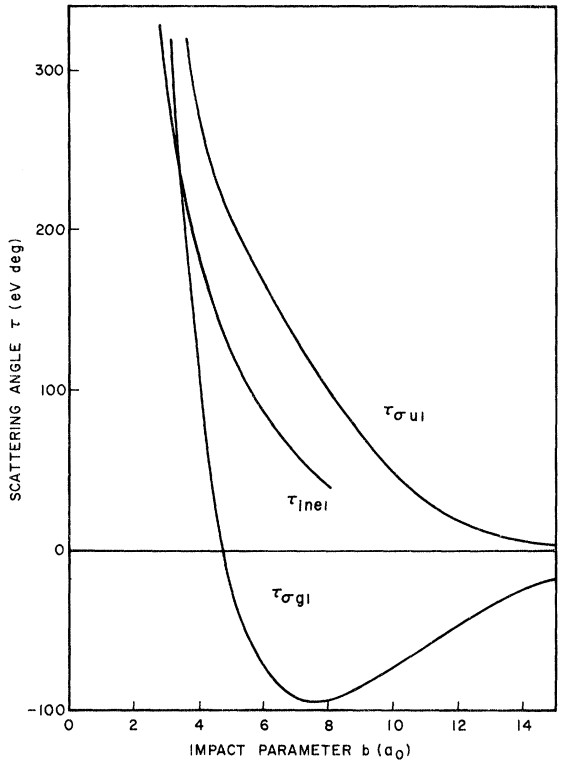

FIG. 2. Reduced scattering angle vs impact parameter for elastic scattering in the σ_{g1} and σ_{u1} states and for inelastic scattering.

Equations (17) and (21) were derived in the small-angle or high-energy approximation, and the explicit energy dependences of ρ and τ were thus artificially removed. This approximation will lead to some error at the lowest experimental energy for large scattering angles.

For the case of $Li^+ + Li$ the initial electronic state with the electron on one nucleus is a linear combination of the two degenerate states σ_{g1} and σ_{u1}. The scattering proceeds through the two channels, and in the final state of both channels the electron is equally likely to sit on either nucleus. Neglecting the interference between the two channels, the reduced elastic cross section is

$$\rho_{el}(\tau) = \tfrac{1}{4}\left[\rho_{\sigma_{g1}}(\tau) + \rho_{\sigma_{u1}}(\tau)\right]. \tag{22}$$

In Fig. 2 we plot the reduced scattering angle $\tau(b)$ versus impact parameter for the σ_{g1} and σ_{u1} states. The attractive region of the σ_{g1} potential at large separations gives rise to a negative scattering angle with a maximum value (rainbow scattering angle) of 94 eV deg. The differential cross sections for the σ_{g1} and σ_{u1} channels and their sum ($= 4\rho_{el}$) are plotted in Fig. 3. The sharp peak at 94 eV deg is the rainbow feature. The smooth bump near 170 eV deg is due to the detailed shape of the σ_{u1} intermolecular potential. For $R > 6a_0$ this potential is Gaussian, leading to a reduced cross section which is constant for small angles and increases slowly as a function of angle. For $R < 6a_0$ the potential is more repulsive than the large-R Gaussian, and this turns the cross section downward. The bump at 440 eV deg in both $\rho_{\sigma_{g1}}$ and $\rho_{\sigma_{u1}}$ is due to the strongly repulsive core-core interaction. This feature of the calculated cross section is sensitive to the choice of core-core interaction and the cross section for $\tau > 400$ eV deg may not be quantitatively correct. The observed rainbow angle[1] of about 80 eV deg is in substantial agreement with the calculation.

B. Semiclassical Approximation

The interference effects between the two channels are included in the semiclassical approximation. According to Ford and Wheeler[5] the scattering amplitude is well approximated by the classical cross section

$$|f_n(\tau)| = \left| \frac{\tau_n b}{(d\tau_n/db)\,\theta \sin\theta} \right|^{1/2}, \tag{23}$$

and the phase of the scattering amplitude is given by the classical action integral, which we write as

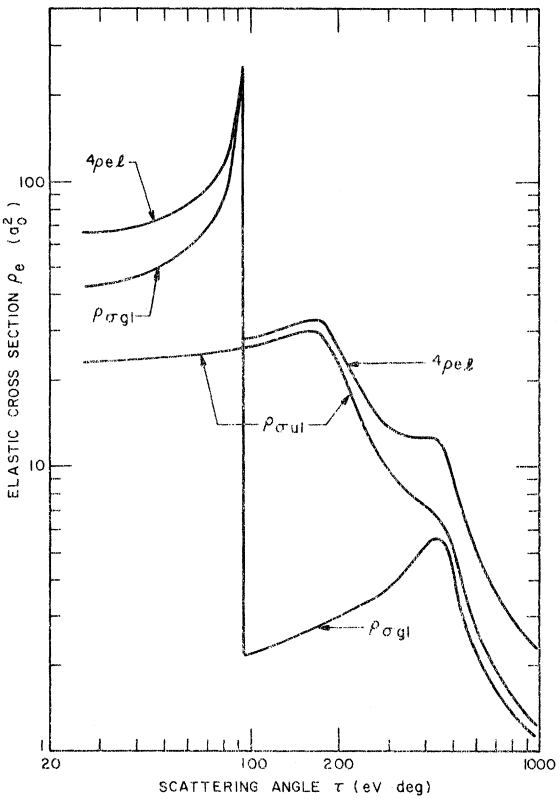

FIG. 3. Classical reduced elastic differential cross section vs reduced scattering angle for the σ_{g1} and σ_{u1} states and their sum, which is four times ρ_{el}, the experimental cross section.

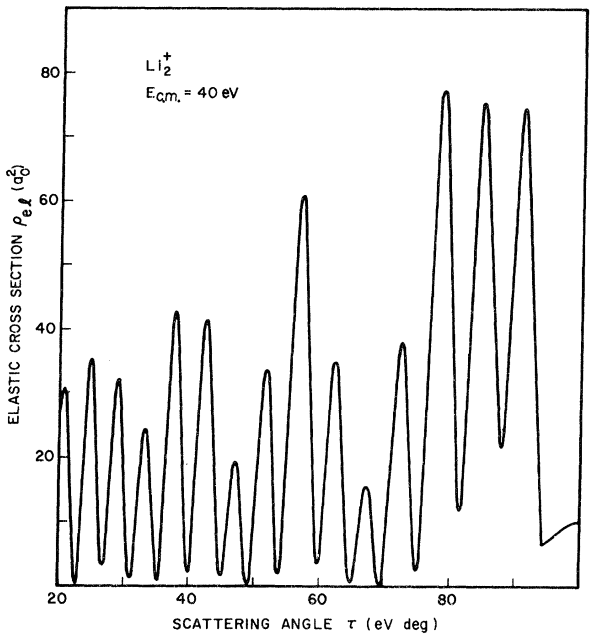

FIG. 4. Semiclassical reduced elastic differential cross section vs reduced scattering angle at 40 eV, showing the interference effects for scattering angles less than the rainbow angle.

$$\beta_n = -\frac{\sqrt{\pi}}{v}\sum_i \frac{c_i^n}{\alpha_i}(1+2\alpha_i^2 b^2)\exp(-\alpha_i^2 b^2) - \tfrac{1}{4}\pi\left[2-\operatorname{sgn}\left(\frac{d\tau}{db}\right)-\operatorname{sgn}(\tau)\right] . \quad (24)$$

The semiclassical cross section is then

$$\rho_{el}(\tau) = \tfrac{1}{4}\left|\sum_n \left|\frac{\tau_n b}{d\tau_n/db}\right|^{1/2} e^{i\beta_n}\right|^2 , \quad (25)$$

where the sum is taken over the classical paths contributing at angle $|\tau|$ for both the σ_{g1} and σ_{u1} states. For $\tau < 94$ eV deg there are three classical paths for the σ_{g1} state. The semiclassical cross section is shown in Fig. 4 for $E_{c.m.} = 40$ eV. The interference pattern is complicated with the slow period due to the interference between the two paths of the σ_{g1} state with the negative scattering angle near the rainbow angle. These oscillations are not observed in the experiment[1] for $\tau < 94$ eV deg although the slow period may be observable with some improvement in resolution. The semiclassical approximation breaks down near the rainbow angle and predicts too abrupt a drop in the cross section at the rainbow angle.

For scattering angles greater than the rainbow angle only one classical path from each quantum state contributes to the elastic differential cross section, and we find

$$\rho_{el}(\tau) = \tfrac{1}{4}\{\rho_{\sigma_{g1}}^{cl} + \rho_{\sigma_{u1}}^{cl} + 2(\rho_{\sigma_{g1}}^{cl}\rho_{\sigma_{u1}}^{cl})^{1/2}\cos[\gamma(\tau)/v]\}. \quad (26)$$

The charge-transfer differential cross section is given by (26) with a negative interference term. The classical cross sections are a function of τ alone, and the relative phase is a function of τ divided by the ion velocity. The semiclassical cross section is plotted in Fig. 5 for $E_{c.m.} = 40$ eV, and the phase function $\gamma(\tau)$ is plotted in Fig. 6. The phase function increases for small angles and then flattens out. Therefore the interference oscillations are rapid for small angles and slow for large angles. However, the magnitude of $\gamma(\tau)$ is large, and for fixed reduced angle τ the cross section oscillates rapidly as a function of ion velocity. The phase function $\gamma(\tau)$ can be mapped out experimentally by measuring the differential cross section as a function of ion velocity for fixed τ. These interference oscillations are present in the experimental data although they were not identified as such. The positions of the maxima and minima in the calculated cross sections agree well with experiment[1] for ion energies between 25 and 100 eV and for scattering angles between about

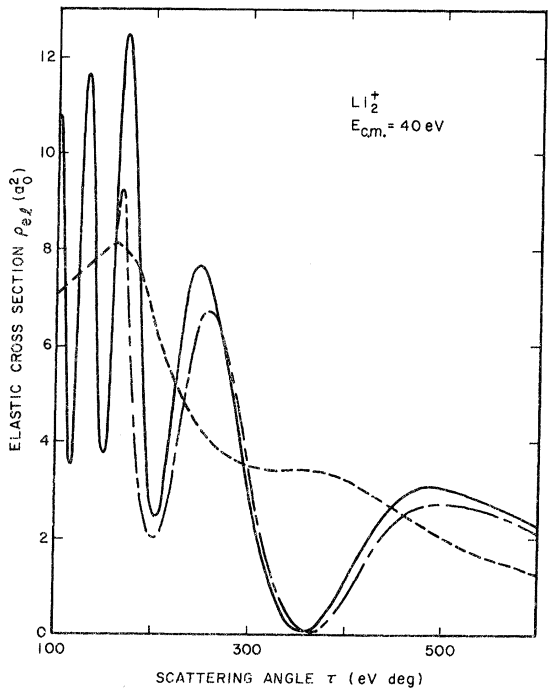

FIG. 5. Semiclassical reduced elastic differential cross section vs reduced scattering angle at 40 eV, showing the interference effects for scattering angles greater than the rainbow angle. Dashed line is the classical cross section which omits the interference effect; in the charge-transfer differential cross section the oscillatory term has the opposite sign. The long dashed line includes the effects of the inelastic channel [Eq. (42)].

200 and 600 eV deg. The magnitude of the experimental oscillations is much smaller than the calculated magnitude. It is desirable to have a thorough experimental study of these oscillations to verify both the form of the phase factor and its calculated magnitude. It appears that the phase factor is in excellent agreement with experiment.

VI. INELASTIC CROSS SECTION

Aberth *et al.*[1] also measured an inelastic cross section $Li^+ + Li \rightarrow Li^+ + Li^*$ in which the Li atom is left in the $2p$ excited state. These authors plot an unnormalized ratio of signals in the $2p$ and elastic channels. This inelastic process goes via transitions at the $\sigma_{u1} - \pi_{u1}$ curve crossing at $R = 5.95a_0$. Within the adiabatic approximation the σ_{u1} and π_{u1} states have different symmetry and there are no transitions. The transitions occur because of the breakdown of this symmetry in the time-dependent problem. A similar problem arises in H_2^+ and has been treated by Bates and Williams.[11]

We again treat the ion motion classically and take one ion at the origin and the other at $X = b$, $Y = 0$, $Z = vt$, $R = (b^2 + v^2t^2)^{1/2}$. We solve the one-electron problem in the time-dependent potentials of the nuclei. The time-dependent Schrödinger equation is

$$\frac{i\partial\Phi(t)}{\partial t} = H_T(t)\Phi(t), \tag{27}$$

where

$$H_T = H + V_{\text{ion-ion}}(R(t)) - E_{\sigma_{g1}}(\infty). \tag{28}$$

We expand the wave function as a linear combination of solutions of the adiabatic problem found in Sec. IV:

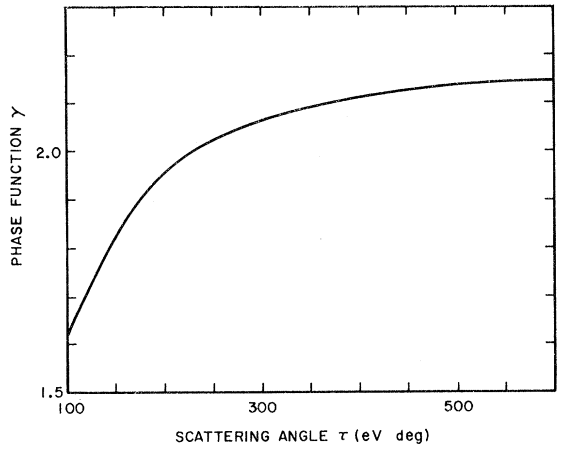

FIG. 6. Phase function [Eq. (26)] vs reduced scattering angle which determines the phase of the interference oscillations for all ion velocities and for scattering angles greater than the rainbow angle.

$$H_T(t)\psi_n(t) = V_n(R(t))\psi_n(t),$$
$$\Phi(t) = \sum_n a_n(t)\psi_n(t)\exp\left[-i\int^t V_n(t')\,dt'\right]. \tag{29}$$

We consider only the two-state problem with the σ_{u1} and π_{u1} states and find the Schrödinger equation

$$\frac{da_\sigma}{dt} = -a_\pi \int \psi_\sigma^* \frac{\partial\psi_\pi}{\partial t}\exp\left[i\int^t (V_\sigma - V_\pi)\,dt'\right],$$
$$\frac{da_\pi}{dt} = -a_\sigma \int \psi_\pi^* \frac{\partial\psi_\sigma}{\partial t}\exp\left[-i\int^t (V_\sigma - V_\pi)\,dt'\right]. \tag{30}$$

The matrix element in this equation is

$$\int \psi_\sigma^* \frac{\partial\psi_\pi}{\partial t} = -\int \psi_\pi^* \frac{\partial\psi_\sigma}{\partial t} = \frac{vbM}{R^2}, \tag{31}$$

where

$$M = \int \psi_\sigma^* \left(z\frac{\partial\psi_\pi}{\partial x} - x\frac{\partial\psi_\pi}{\partial z}\right) d^3r. \tag{32}$$

In this integral the internuclear axis is in the z direction and the π orbital is directed in the x direction. The matrix element M is a function of R and can be calculated by performing the integral (32) numerically using the wave functions found in Sec. IV. We find $M^2 = 0.64$, 0.68, and 0.72 for $R = 4$, 6, and $8a_0$, respectively, which is essentially constant. In what follows we take $M = (0.68)^{1/2} = 0.825$.

We find the phase factor in (30) by expanding $V_\sigma - V_\pi$ about the level crossing separation R_0:

$$V_\sigma - V_\pi = (R - R_0)\,V',$$
$$V' = \frac{d}{dR}(V_\sigma - V_\pi)\big|_{R=R_0}, \tag{33}$$

and perform the t' integration to find

$$\varphi(s) \equiv \int_0^t (V_\sigma - V_\pi)\,dt'$$
$$= \frac{V'}{v}\left[\frac{s(b^2+s^2)^{1/2}}{2} + \frac{b^2}{2}\ln\left(\frac{s+(b^2+s^2)^{1/2}}{b}\right) - R_0 s\right], \tag{34}$$

where $s = vt$. The time-dependent Schrödinger equation now reads

$$\frac{da_\sigma(s)}{ds} = -\frac{bM}{b^2+s^2}a_\pi(s)\,e^{i\varphi(s)},$$
$$\frac{da_\pi(s)}{ds} = \frac{bM}{b^2+s^2}a_\sigma(s)\,e^{-i\varphi(s)}, \tag{35}$$

with the boundary conditions

$$a_\sigma(-\infty) = 1, \quad a_\pi(-\infty) = 0. \tag{36}$$

We want to solve (35) for a_σ and a_π to find the transition probability

$$P_{\sigma\pi}(b) = |a_\pi(\infty)|^2. \tag{37}$$

One's first thought is to use time-dependent perturbation theory to solve (35). When this is done

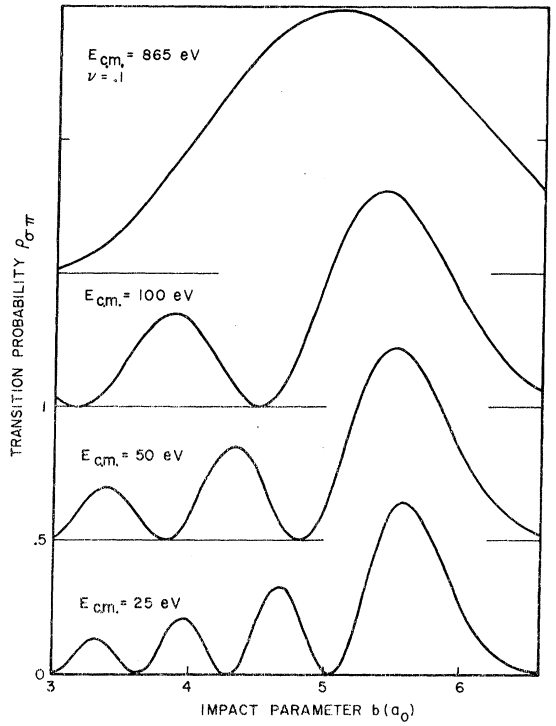

FIG. 7. Transition probability $\sigma_{u1} \rightarrow \pi_{u1}$ vs impact parameter for four ion energies (center of mass).

for the experimental range of energies one finds transition probabilities greater than unity, so that it is necessary to find a more accurate method of solving the equations. We have solved (35) by integrating the differential equations numerically. Care must be taken to treat the rapidly varying phase factor $\varphi(s)$ accurately but, when this is done, numerical integration works satisfactorily. We find $V' = -0.021$ by fitting $V_\sigma - V_\pi$ for $3 < R < 7$, and we take $R_0 = 5.95a_0$ and $M = 0.825$. The calculated transition probabilities versus impact parameter are shown in Fig. 7 for several values of ion energy.

For $b < R_0$ the system passes through the level crossing twice and transitions occur during both passes. There is a quantum-mechanical interference effect between the two transition amplitudes which depends on the phase difference generated between the two transitions. The phase difference is

$$\delta\varphi = +\varphi[(R_0^2 - b^2)^{1/2}] - \varphi[-(R_0^2 - b^2)^{1/2}]$$

$$= -\frac{V'}{v}\left[R_0(R_0^2 - b^2)^{1/2} - b^2 \ln\left(\frac{R_0 + (R_0^2 - b^2)^{1/2}}{b}\right)\right] . \quad (38)$$

The transition amplitudes interfere constructively, and the transition probability is maximum when $\Delta\varphi = 2\pi(n + \frac{1}{4})$, where $n = 0, 1, 2, \ldots$, and the amplitudes interfere destructively, and $P_{\sigma\pi}$ vanishes when $\delta\varphi = 2\pi(n + \frac{3}{4})$.

In the inelastic scattering channel the ion comes in on the σ_{u1} curve and goes out on the π_{u1} curve. The reduced scattering angle is then (see Fig. 2)

$$\tau_{\text{inel}}(b) = \tfrac{1}{2}[\tau_{\sigma_{u1}}(b) + \tau_{\pi_{u1}}(b)] . \quad (39)$$

This is a classical expression for the scattering angle which assumes a definite potential curve for the ion. For R near the curve-crossing radius the valence electron is hopping between the σ and the π states and there is no definite potential. Equation (39) is an approximation which we do not know how to correct. Within this approximation the reduced inelastic cross section is

$$\rho_{\text{inel}}(\tau) = \tfrac{1}{4}\tau_{\text{inel}}\, b\, P_{\sigma\pi}(b)\left(\frac{d\tau_{\text{inel}}}{db}\right)^{-1} . \quad (40)$$

This cross section is plotted in Fig. 8 for the three experimental energies $E_{\text{c.m.}} = 25$, 50, and 100 eV. The experimental[1] "ratio of signals in the $2p$ and the elastic channel at each angle" is plotted for $E_{\text{c.m.}} = 25$ eV on the same figure. One can only compare the positions of the peaks and valleys,

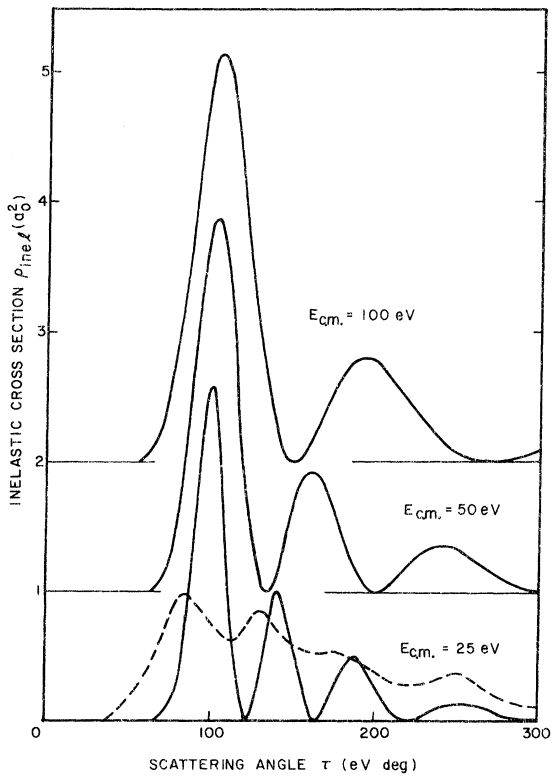

FIG. 8. Reduced inelastic differential cross section vs reduced scattering angle for the three ion energies used experimentally. Dashed line is the experimental "ratio of signals in the $2p$ and elastic channels" from Ref. 1.

since the experimental data are given as a ratio of cross sections with unspecified normalization. As seen in Fig. 8 the agreement in peak positions is reasonably good at 25 eV; the agreement is comparable at 50 and 100 eV. The position of the first peak is at a reduced scattering angle of about 85 eV deg experimentally and about 100 eV deg theoretically. In the calculation the position of the first peak is determined primarily by the level crossing radius and the potential curves and is less sensitive to the approximations involved in Eqs. (33) and (39) than the positions of the higher peaks. A more detailed comparison with experiment will have to wait until absolute cross section measurements are available.

The total (non-charge-transfer) inelastic cross section is found by integrating $P_{\sigma\pi}(b)$ over the impact parameter:

$$\sigma_{\text{inel}} = \tfrac{1}{2}\pi \int_0^\infty P_{\sigma\pi}(b)\, b\, db \ . \tag{41}$$

This cross section is plotted versus ion velocity in Fig. 9. Since in the final state $\psi_{\pi_{u1}}$ the electron is equally likely to sit on either ion, the total charge-transfer inelastic cross section is equal to the total non-charge-transfer inelastic cross section.

The inelastic process removes particles from the σ_{u1} channel and the elastic cross section (26) is modified to read

$$\rho_{el}(\tau) = \tfrac{1}{4}\{\rho_{\sigma_{g1}}(\tau) + \rho_{\sigma_{u1}}(\tau)\,[1 - P_{\sigma\pi}(b)] + 2\{\rho_{\sigma_{g1}}\rho_{\sigma_{u1}}[1 - P_{\sigma\pi}(b)]\}^{1/2} \times \cos[\gamma(\tau)/v + \varphi']\} \ , \tag{42}$$

where φ' is the phase of $a_g(\infty)$; this phase shift is small and unimportant. The modified classical

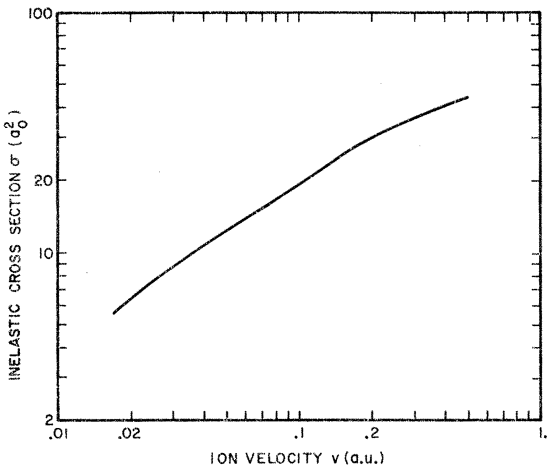

FIG. 9. Total inelastic (non-charge-transfer) cross section vs ion velocity.

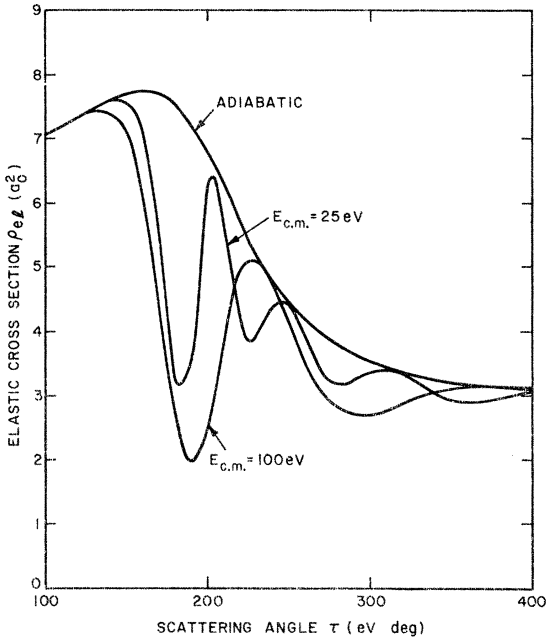

FIG. 10. Reduced elastic differential cross section vs reduced scattering angle within the adiabatic approximation and with corrections for the inelastic process.

cross section, neglecting the interference term, is plotted in Fig. 10 for $E_{\text{c.m.}} = 25$ and 100 eV and is compared with the adiabatic approximation of Sec. V. The classical elastic cross section has a deep minimum at $\tau = 190$ eV deg and oscillates for larger angles. This effect occurs in the same region of scattering angle since the interference oscillations and the periods of oscillation are similar. The modified semiclassical elastic cross section, containing both the interference oscillations and the inelastic effect, is shown as the long dashed line in Fig. 5 for $E_{\text{c.m.}} = 40$ eV. We see that the interference oscillations are the dominant effect and that the modifications due to the inelastic channel are small. This supports the statement that the observed oscillations are due to the interference oscillations rather than the inelastic channel.

VII. CHARGE-TRANSFER CROSS SECTION

The charge-transfer total cross section for the process

$$Li^+ + Li \rightarrow Li + Li^+$$

has been measured as a function of ion velocity by Perel *et al.*[3] What is measured is the total cross section, including elastic and inelastic processes. This cross section has been calculated by Peek *et al.*[12] within the adiabatic approximation using intermolecular potentials calculated by Michels. In this section we calculate the charge-transfer cross section, using the intermolecular potentials found

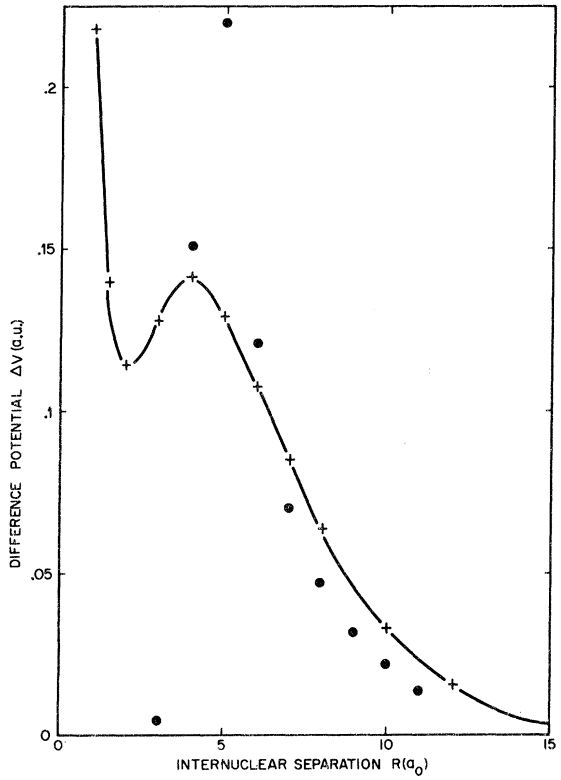

FIG. 11. $\sigma_{u1} - \sigma_{g1}$ difference potential used in the charge-transfer cross section vs internuclear separation. Crosses are the present calculation and the solid line is the Gaussian fit to the crosses. Solid circles are the potential due to Michels and used in a previous calculation.

in Sec. IV, making use of two approximations. First we use the adiabatic approximation which should be valid for small ion velocities. Second, we use a three-state approximation which takes into account the inelastic transition at the σ_{u1}-π_{u1} curve crossing. This approximation should be valid for higher ion velocities than the adiabatic approximation, but should break down for sufficiently high ion velocity, owing to the excitation of higher states.

A. Adiabatic Approximation

We continue the discussion of the time-dependent Schrödinger equation of Sec. VI. In the initial state the electron sits on the ion at the origin and the wave function is

$$\Phi(-\infty) = (1/\sqrt{2})(\psi_{\sigma_{g1}} + \psi_{\sigma_{u1}}) . \tag{43}$$

In the final state the electron sits on the moving ion:

$$\Phi_f = (1/\sqrt{2})(\psi_{\sigma_{g1}} - \psi_{\sigma_{u1}}) . \tag{44}$$

Within the adiabatic approximation the amplitudes $a_n(t)$ in Eq. (29) are constant and the time development of the wave function is determined by the phase factors

$$\Phi(t) = (1/\sqrt{2})\psi_{\sigma_{g1}} \exp(-i\int_{-\infty}^{t} V_{\sigma_{g1}} dt) + (1/\sqrt{2})\psi_{\sigma_{u1}} \exp(-i\int_{-\infty}^{t} V_{\sigma_{u1}} dt) . \tag{45}$$

The overlap with the final state is then

$$\langle \Phi_f | \Phi(\infty) \rangle = \tfrac{1}{2}[\exp(-i\int_{-\infty}^{\infty} V_{\sigma_{g1}} dt) - \exp(-i\int_{-\infty}^{\infty} V_{\sigma_{u1}} dt)] , \tag{46}$$

and the charge-transfer probability is

$$P_{ct}(b) = |\langle \Psi_f | \Psi(\infty) \rangle|^2 = \tfrac{1}{2}[1 - \cos\Delta\varphi(b)] , \tag{47}$$

where

$$\Delta\varphi(b) = \int_{-\infty}^{\infty} (V_{\sigma_{u1}} - V_{\sigma_{g1}}) dt . \tag{48}$$

Writing the difference potential as a sum of Gaussians (found by a least-squares fit)

$$\Delta V(R) = V_{\sigma_{u1}}(R) - V_{\sigma_{g1}}(R) = \textstyle\sum_i c_i e^{-(\alpha_i R)^2} , \tag{49}$$

we find

$$\Delta\varphi(b) = \sum_i c_i \frac{\sqrt{\pi}}{\alpha_i v} \exp(-\alpha_i^2 b^2) , \tag{50}$$

where v is the ion velocity. Equations (47)–(50) are equivalent to the conventional expression for the charge-transfer probability.[13]

In Fig. 11 we show the difference potential. The crosses are the calculated points taken from Sec. IV. The solid line is the sum of Gaussians fitted to the calculated points. The parameters of the Gaussian fit are given in Table IV. The solid circles are the difference potential calculated by Michels[12] and used in the previous calculation[12] of the cross section. Our difference potential is about 50% larger than Michels's for large separations and behaves qualitatively differently for small separation. The phase difference $\Delta\varphi(b)$ is plotted in Fig. 12 for $v = 0.1$ and the charge-transfer probability $P_{ct}(b)$ is shown in the upper half of Fig. 13, again for $v = 0.1$.

The physical picture of the charge-transfer process is as follows.[13] Initially the electron sits in the 2s state of the target atom, which is degenerate with the 2s state of the moving ion. As the ions approach there is an increasing matrix element between these two states, which causes them to split

TABLE IV. Parameters (in a.u.) of the least-squares Gaussian fit [Eq. (49)] to the difference potential.

c_i	α_i
0.0927	0.12
0.1463	0.16
−0.0537	0.25
−0.2603	0.45
0.3660	0.7
0.1231	1.3

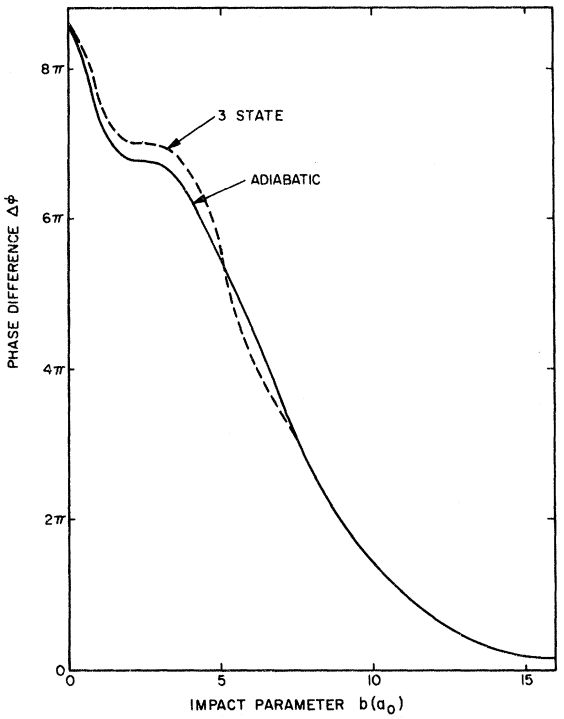

FIG. 12. Phase difference between the σ_{g1} and σ_{u1} states vs impact parameter within the adiabatic and three-state approximations.

apart. The electron is no longer in a stationary state and it begins to transfer from one atom to the other and back again with a period $\Delta t = 2\pi\hbar/\Delta V(R)$. This transfer process is terminated as the ions move apart. Referring to Fig. 13 for ion velocity $v = 0.1$ and an impact parameter $b = 11$, the electron has enough time during the collision to transfer to the moving ion but not enough time to begin the transfer back. For $b = 9$ the ions approach more closely, the difference potential becomes larger, and the electron transfer takes place more rapidly; the electron has transferred to the moving ion and back to the target ion during the collision. Because of this resonance behavior the charge-transfer probability oscillates between 0 and 1 as a function of b. The total charge-transfer cross section is just the integral over impact parameter of the charge-transfer probability:

$$\sigma_{ct}(v) = 2\pi \int_0^\infty P_{ct}(b)\, b\, db \ . \qquad (51)$$

The charge-transfer cross section is plotted in Fig. 14 and compared with experiment.[3] The magnitude of the cross section is determined by the impact parameter (the Firsov[14] radius) at which the phase difference drops to a small fraction of π. The oscillatory term in the cross section arises from the anomaly in the phase difference $\Delta\varphi(b)$ near $b = 3a_0$ which is itself due to the wiggle in the difference potential. Note that the phase difference does not go through an extremum[13] but that it is approximately flat near $b = 2.5a_0$.

Perhaps it is worthwhile to comment, at this point, on the use of a classical expression for the total cross section and a semiclassical expression for the differential cross section. In the expression for the differential scattering cross section (25) one permits the waves from the σ_{g1} and σ_{u1} states to interfere at the same scattering angle, that is, for different impact parameters. However, in the classical calculation of the total cross section, one permits the waves from the σ_{g1} and σ_{u1} states to interfere at the same impact parameter; one then integrates over impact parameter. Since the total cross section is just the integral over angles of the differential cross section, it appears that we have two physically different expressions for the total cross section. The question arises, are the two expressions different, and if so, which one is correct.

In order to resolve this point, we have to go back to the quantum-mechanical expression for the charge-transfer scattering amplitude[4]:

$$f(\theta) = \frac{1}{4ik} \sum_{l=0}^{\infty} (2l+1)\, [\exp(2i\delta_l^g) - \exp(2i\delta_l^u)]\, P_l(\cos\theta) \ . \qquad (52)$$

It is from this expression that Ford and Wheeler[5] derive the semiclassical scattering amplitude by making use of WKB phase shifts, replacing $\sum_l$ by

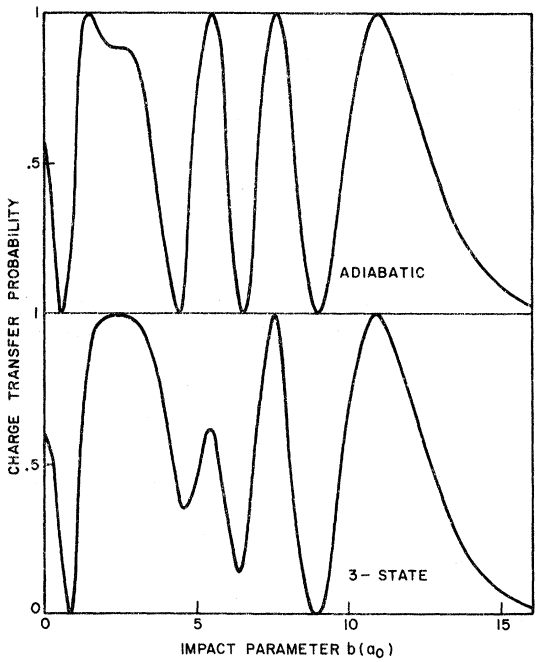

FIG. 13. Charge-transfer probability vs impact parameter for $v = 0.1$ within the adiabatic and three-state approximations.

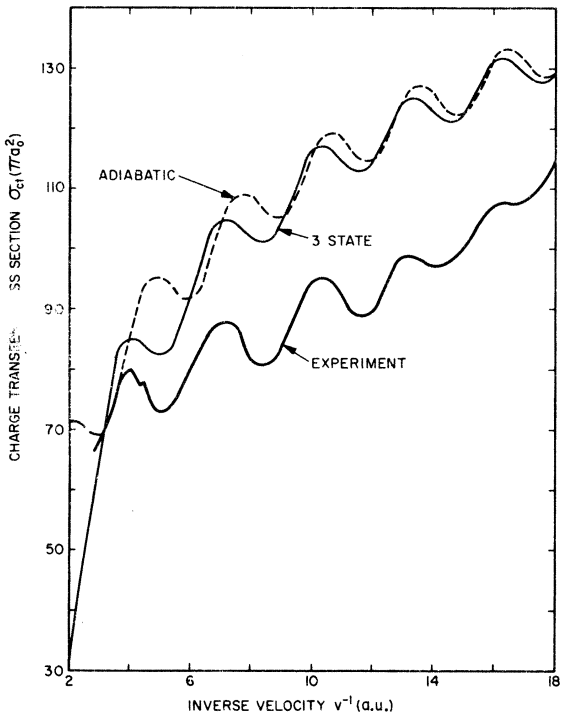

FIG. 14. Total charge-transfer cross section vs ion velocity within the adiabatic and three-state approximation compared with the experimental cross section of Perel *et al.* (Ref. 3).

$\int dl$ and performing the integration by the method of stationary phase. Quantum mechanically, the total cross section is

$$\sigma = \frac{\pi}{4k^2} \sum_{l=0}^{\infty} (2l+1) \left| \exp(2i\delta_l^g) - \exp(2i\delta_l^u) \right|^2 . \quad (53)$$

The WKB phase shift at high energy, $V/E \ll 1$, is

$$\delta_l^n = -\int_{-\infty}^{\infty} \frac{V(R)\,dz}{2v} = -\frac{\sqrt{\pi}}{2v} \sum_i \frac{c_i^n}{\alpha_i} \exp(-\alpha_i^2 b^2). \quad (54)$$

Making the usual correspondence $kb = l + \frac{1}{2}$ and replacing $\sum_l$ by $\int kdb$, we find precisely the classical expression (51) for the total cross section. Thus the classical expression for the total charge-transfer cross section is correct and one has the choice in the calculation of allowing the two waves to interfere either at the same impact parameter or at the same scattering angle. It is more convenient to use the classical expression (51) than to go through the intermediate differential cross section calculation. In fact, one cannot use the semiclassical differential cross section to compute the total cross section because it fails for small scattering angle, and the integral diverges.

B. Three-State Approximation

The adiabatic approximation neglects the inelastic transitions at the $\sigma_{\mu 1} - \pi_{\mu 1}$ curve crossing which we know are important even for relatively small ion velocities. In order to include the inelastic processes we solve the time-dependent Schrödinger equation (27) in the three-state approximation, keeping only the σ_{g1}, $\sigma_{\mu 1}$, and $\pi_{\mu 1}$ states in the wave function expansion (29). The time-dependent wave function is

$$\begin{aligned}\Phi(t) = {} & (1/\sqrt{2})\,\psi_{\sigma_{g1}} \exp(-i\int_{-\infty}^{t} V_{\sigma_{g1}}\,dt) \\ & + (1/\sqrt{2})\,a_{\sigma_{u1}}(t)\,\psi_{\sigma_{u1}} \exp(-i\int_{-\infty}^{t} V_{\sigma_{u1}}\,dt) \\ & + (1/\sqrt{2})\,a_{\pi_{u1}}(t)\,\psi_{\pi_{u1}} \exp(-i\int_{-\infty}^{t} V_{\pi_{u1}}\,dt) , \end{aligned} \quad (55)$$

where $a_{\sigma_{u1}}(t)$ and $a_{\pi_{u1}}(t)$ were calculated in Sec. VI. We have two final states with the electron in a $2s$ or $2p$ atomic state on the moving ion:

$$\begin{aligned} \Phi_{f_{2s}} &= (1/\sqrt{2})\,(\psi_{\sigma_{g1}} - \psi_{\sigma_{u1}}) , \\ \Phi_{f_{2p}} &= (1/\sqrt{2})\,(\psi_{\pi_{g1}} - \psi_{\pi_{u1}}) , \end{aligned} \quad (56)$$

so that the total charge-transfer probability is

$$P_{ct}(b) = \tfrac{1}{2}\{1 - \mathrm{Re}[a_{\sigma_{u1}}(\infty)\, e^{-i\Delta\varphi(b)}]\}, \quad (57)$$

with $\Delta\varphi(b)$ given by (50). Both the phase and the amplitude of $a_{\sigma_{u1}}(\infty)$ are affected by the curve crossing. The total phase of this interference term is plotted as a dashed line in Fig. 12 for $v = 0.1$. The $\sigma - \pi$ transition probability $P_{\sigma\pi}(b)$ for $v = 0.1$ is plotted in Fig. 7 and the amplitude of $a_{\sigma_{u1}}(\infty)$ is $[1 - P_{\sigma\pi}(b)]^{1/2}$. For $v = 0.1$, this amplitude is unity for large b, drops to ~ 0.1 for $b = 5$, and rises to near unity for small b. The charge-transfer probability for $v = 0.1$ in the three-state approximation is plotted in Fig. 13 for comparison with the adiabatic approximation. There is a small shift in the oscillation due to the phase difference in Fig. 12; the magnitude of the oscillation is reduced near $b = 5$ due to the reduction in the amplitude of $a_{\sigma_{u1}}(\infty)$. The total charge-transfer cross section calculated from (51) is plotted in Fig. 14. At low ion velocity the three-state approximation approaches the adiabatic approximation, as it should. The magnitude of the cross section is almost unaffected by the inelastic process. This magnitude is determined by the scattering at large impact parameter near the Firsov radius $b \sim 15\,a_0$, whereas the inelastic process goes only for smaller impact parameters $b < 7a_0$. However, the oscillatory term in the cross section is affected for high ion velocity. The phase of the oscillatory term is changed without much effect on its amplitude. The positions of the maxima and minima of the charge-transfer cross section in the three-state approximation are in excellent agreement with experiment,[3] and the magnitude of the oscillations agrees pretty well. The oscillatory term depends on the difference potential for $R \lesssim 6a_0$ and also on the treatment of the inelastic process and the good agreement with ex-

periment tends to confirm these features of the calculation. The absolute magnitude of the theoretical cross section is 25% larger than experiment at low velocity, and this discrepancy decreases at higher velocities. The magnitude of the cross section depends on the difference potential for large internuclear separation $R > 10a_0$. The relative accuracy of the difference potential is less at large R where the difference potential is small. The uncertainty in ΔV at $R = 15a_0$ is $\pm 10\%$, and the uncertainty in the theoretical cross section is $\pm 5\%$. The stated experimental uncertainty is $\pm 15\%$. Michels's potential, which is considerably smaller than ours for large R, yields a cross section whose magnitude is in good agreement with experiment.

VIII. CONCLUSIONS

To review, we have set up a one-electron effective Hamiltonian for Li_2^+ and have found the six lowest eigenvalues as a function of internuclear separation. The numerical method used is economical and accurate and may find application in other one-electron problems. The intermolecular potentials, together with one matrix element, were used to calculate absolute cross sections for three scattering processes which have been measured. Qualitatively, the theoretical model explains all the observed features of the cross sections. In particular, the observed level crossing[1] is identified as a crossing of the σ_{u1} and π_{u1} levels. Where a quantitative comparison is possible, the calculated cross sections agree with experiment within the author's assessment of possible experimental error. There are sound theoretical reasons for believing that the theoretical model, simple though it is, is an accurate physical model for Li_2^+ for $R > 2a_0$. It is therefore desirable to have accurate experimental measurements to test the theory. It is desirable to have (a) absolute elastic cross sections over a wider range of energies with a careful study of the interference term, (b) absolute inelastic cross sections in order to compare the magnitude and shape of the curves, and (c) a more accurate absolute measurement of the charge-transfer cross section.

The theoretical methods used here can be applied to the other symmetric or asymmetric alkali molecular ions and to the alkali-hydride molecular ions.

[1]W. Aberth, O. Bernardini, D. Coffey, Jr., D. C. Lorents, and R. E. Olson, Phys. Rev. Letters 24, 345 (1970).
[2]D. C. Lorents, G. Black, and O. Heinz, Phys. Rev. 137, A1049 (1965).
[3]J. Perel, H. L. Daley, J. M. Peek, and T. A. Green, Phys. Rev. Letters 23, 677 (1969).
[4]H. S. W. Massey and R. A. Smith, Proc. Roy. Soc. (London) A142, 142 (1933).
[5]K. W. Ford and J. A. Wheeler, Ann. Phys. (N. Y.) 7, 259 (1959).
[6]R. P. Marchi and F. T. Smith, Phys. Rev. 139, A1025 (1965).
[7]C. E. Moore, *Atomic Energy Levels*, Natl. Bur. Std. (U.S.) Circ. No. 467 (U.S. GPO, Washington, D. C., 1949).
[8]J. C. Slater, Phys. Rev. 32, 349 (1928).
[9]C. R. Fischer and P. J. Kemmey, Phys. Rev. 186, 272 (1969).
[10]F. T. Smith, R. P. Marchi, and K. G. Dedrick, Phys. Rev. 150, 79 (1966).
[11]D. R. Bates and D. A. Williams, Proc. Phys. Soc. (London) 83, 425 (1964).
[12]J. M. Peek, T. A. Green, J. Perel, and H. M. Michels, Phys. Rev. Letters 20, 1419 (1968).
[13]J. Perel, Phys. Rev. A 1, 369 (1970).
[14]O. B. Firsov, Zh. Eksperim. i Teor. Fiz. 21, 1001 (1951).

PHYSICAL REVIEW A VOLUME 4, NUMBER 1 JULY 1971

Fine Structure and Diamagnetic Zeeman Effect in He ($4\,^3P$)

T. A. Miller and R. S. Freund
Bell Telephone Laboratories, Murray Hill, New Jersey 07974
(Received 16 September 1971)

The $4\,^3P$ state of helium has been excited and aligned by electron impact in a strong magnetic field. Transitions between Zeeman levels of the fine-structure states are induced by microwave frequency radiation and are detected through the resulting change in polarization of 3188-Å fluorescence. The derived values of the fine-structure intervals are $4\,^3P_0$-$4\,^3P_1$ $= 3306.6 \pm 1.0$ MHz and $4\,^3P_1$-$4\,^3P_2 = 270.7 \pm 0.8$ MHz. The diamagnetic Zeeman interaction produces an observable effect, and the magnitude of its anisotropic part has been measured. The atomic radius and quadrupole moment are derived from this measurement and agree within experimental error with the values for a hydrogenic $4p$ orbital.

I. INTRODUCTION

Accurate measurements of the fine structure of helium $2\,^3P$ and $3\,^3P$ have been carried out for many years,[1–10] both for the purpose of testing higher-order corrections to calculated He wave functions